ARTICLE IN PRESS

Journal of Fluids and Structures xxx (xxxx) xxx

Contents lists available at ScienceDirect

Journal of Fluids and Structures

journal homepage: www.elsevier.com/locate/jfs

Control of vortex shedding from a circular cylinder surrounded by eight rotating wake-control cylinders at Re=100

G.R.S. Assi [a,*], R.M. Orselli [b], M. Silva-Ortega [c]

[a] Department of Naval Architecture & Ocean Engineering, EPUSP, University of São Paulo, São Paulo SP, Brazil
[b] Department of Aerospace Engineering, Federal University of ABC, São Bernardo do Campo SP, Brazil
[c] Department of Naval Architecture, Universidad Veracruzana, Veracruz, Mexico

ARTICLE INFO

Article history:
Received 29 October 2018
Received in revised form 4 February 2019
Accepted 4 March 2019
Available online xxxx

Keywords:
Vortex shedding
Wake control
Rotating cylinders
Drag reduction

ABSTRACT

The present work investigates the suppression of vortex shedding of a circular cylinder of diameter D surrounded by a polar array 8 rotating wake-control cylinders of a considerably smaller diameter $d/D = 0.05$. A numerical approach was employed to simulate the laminar flow at a Reynolds number of 100. The governing equations were discretised by the finite volume method for a two-dimensional computational domain. The main varying parameter was the rotation speed of the control cylinders, measured as a fraction of the incoming flow speed. A controlled wake (one without alternating vortices) was achieved when the tangential velocity at the surface of the control cylinders was greater than 3 times the free stream velocity. A significant reduction of the overall drag coefficient and mitigation of the unsteady hydrodynamic forces acting on the system were observed as rotation was increased. Given enough rotation, a negative mean drag (thrust) was achieved. The power spent to rotate the 8 control cylinders appeared to be higher than the power-loss associated with the mean drag of a bare cylinder. While still working with an active, open-loop control system, this investigation supports the development of a closed-loop wake-control device for offshore applications.

1. Introduction

It is well known that bluff bodies immersed in a flow will develop a periodic wake of alternating vortices (called the *Karman street*) shed from the separated shear layers and convected further downstream (Bearman, 1984). Control over the vortex-shedding phenomenon has been investigated for decades, gaining special attention after a general physical mechanism for the formation of vortices was proposed by Gerrard (1966). Mostly aiming at reattaching the separated flow or removing the periodicity of the wake, researchers have proposed various techniques to achieve wake control. Some of these appeared as fairings (attempting to streamline the flow around the body), while others came about as interesting contraptions attached or installed around the bluff body to interact with the separated shear layers (for example, Assi et al., 2009, 2010).

It is widely accepted that if the wake is controlled and the shedding of vortices is eliminated the bluff body will not only generate considerably less drag but may also become invulnerable to vortex-induced vibrations (VIV). The present investigation is motivated by the development of novel solutions to suppress VIV from slender bluff structures without

* Corresponding author.
E-mail address: g.assi@usp.br (G.R.S. Assi).

https://doi.org/10.1016/j.jfluidstructs.2019.03.003
0889-9746/

causing excessive drag (perhaps achieving drag reduction) and producing useful forces for dynamic positioning. In the present work, however, we shall refer only to the suppression of the vortex-shedding mechanism as a step towards the suppression of VIV. For reviews on the topic, please follow Zdravkovich (1981) or the recent compilation of Rashidi et al. (2016).

Passive wake-suppression methods rely on modifications of the bluff body geometry to affect the formation and shedding mechanism of vortices (Choi et al., 2008). They require no external energy supply to the fluid–structure system and have a much simpler implementation, which favours their use over the active methods in most engineering applications. In an effort to study a passive control device by employing interfering control rods, Strykowski and Sreenivasan (1990) have reported that the vortex shedding past a circular cylinder can be controlled over a limited range of Reynolds number (Re) by the proper placement of a smaller control rod close to the main cylinder. Wu et al. (2012), Jimenez-Gonzalez and Huera-Huarte (2017) and Silva-Ortega and Assi (2017a, 2018) went on to investigate the passive suppression of VIV of circular cylinders by fitting multiple control rods around their circumference.

Active open- and closed-loop control techniques have received extensive attention by the scientific community (Gad-El-Hak, 2000; Cattafesta and Sheplak, 2011; Schulmeister, 2012; Silva-Ortega and Assi, 2017b), as they can be directly applied or inspire the development of more efficient passive control methods. Among the great variety of active control methods, the *moving surface boundary-layer control* (MSBC) technique relies on the injection of momentum in the boundary layers of the body by rotating small elements placed within or very near the boundary layers around the separation points (Modi, 1997). Rotating elements are usually small circular cylinders placed inside or just above the wall. It is believed that the injection of momentum postpones the effects of the adverse pressure gradient generated by the geometry of the bluff body, moving the separation points to a more advanced position. As a result, the wake becomes narrower and the recirculation region behind the body is suppressed or drastically reduced. One of the most important control parameters directly associated with the injection of momentum is the ratio between the tangential velocity of the moving surface and the flow velocity (U_c/U).

MSBC can be applied as an active open- or closed-loop control. Patnaik and Wei (2002) numerically simulated the flow around a D-section cylinder with MSBC at $Re = 200$ and 400 and verified a recirculation free zone in the wake for $U_c/U = 1.25$. Muddada and Patnaik (2010) made further developments to this control strategy, employing a cylinder fitted with two simple rotary type mechanical actuators located at 120° from the frontal stagnation point. The effectiveness of the MSBC in reducing drag was shown in all tested cases. Mittal and Raghuvanshi (2001) verified this phenomenon employing a numerical approach and observed that two control cylinders provided a local favourable pressure gradient in the wake region, thereby locally stabilising the shear layers. Following that, Mittal (2001) applied the MSBC to control the flow around a circular cylinder in two-dimensional numerical simulations at $Re = 100$ and 10,000. At $Re = 100$ and $U_c/U = 5$, the wake was suppressed; at $Re = 10{,}000$ the wake did not reach a steady state, but it appeared highly organised and narrower when compared to the case without any control. The effect of the gap between the control cylinders and the wall of the main cylinder at $Re = 10{,}000$ was later investigated by Mittal (2003). Recently, Schulmeister et al. (2017) performed experiments at $Re = 47{,}000$ that showed considerable drag reduction for two rotating control cylinders strategically located around the main body. Their numerical simulations at $Re = 500$ revealed interesting details of the reattachment of the flow around the control cylinders.

Korkischko and Meneghini (2012) performed an experiment employing MSBC with 2 control cylinders as a means to suppress VIV of an isolated cylinder mounted on an elastic base with one degree of freedom in the cross-flow direction. VIV suppression was achieved given enough rotation of the control cylinders. Later, Zhu et al. (2015) performed numerical simulations of VIV in two degrees of freedom employing 2 rotating control cylinders for Re between 1,000 and 6,500; in another study (Zhu and Gao, 2017), the effect of the rotation direction was investigated. Recently, MSBC with more than 2 control cylinders has also been tested as a means to suppress vortex shedding of static cylinders as well as VIV of oscillating bodies in the experiments performed by Silva-Ortega and Assi (2018).

2. Objective

The present study investigated if a polar array of 8 rotating wake-control cylinders of a smaller diameter d, equally spaced about a main circular cylinder of a larger diameter D and positioned away from the main cylinders's wall (as defined in Fig. 1), was able to control the wake and suppress vortex shedding. This is part of a wider investigation that started with 2 and 4 control cylinders, not discussed here for brevity, but reported in Silva-Ortega and Assi (2017a, 2018). From those previous works, the arrangement with 8 control cylinders started to present useful characteristics of an omnidirectional device.

The gap (G/D) separating the control cylinders from the main cylinder and the rotation speed of the control cylinders (U_c/U, defined as the ratio between the tangential velocity on the wall of the control cylinders to the speed of the incoming flow) were the main parameters of the investigation: U_c/U varied between 0 and 6, while $G/D = 0.1$ and $d/D = 0.05$ were kept constant. Other works have considered variations in these parameters as well (Silva-Ortega, 2015). As seen in Fig. 1, the control cylinders at the top rotate in the clockwise direction, while the control cylinders at the bottom rotate in the counter-clockwise direction. The system is considered an open-loop, active MSBC device.

The investigation was conducted by means of two-dimensional numerical simulations of the flow at $Re = 100$ ($Re = UD/\nu$, based on the free stream velocity U, the diameter D of the main cylinder and the viscosity ν of the fluid).

Please cite this article as: G.R.S. Assi, R.M. Orselli and M. Silva-Ortega, Control of vortex shedding from a circular cylinder surrounded by eight rotating wake-control cylinders at Re=100. Journal of Fluids and Structures (2019), https://doi.org/10.1016/j.jfluidstructs.2019.03.003.

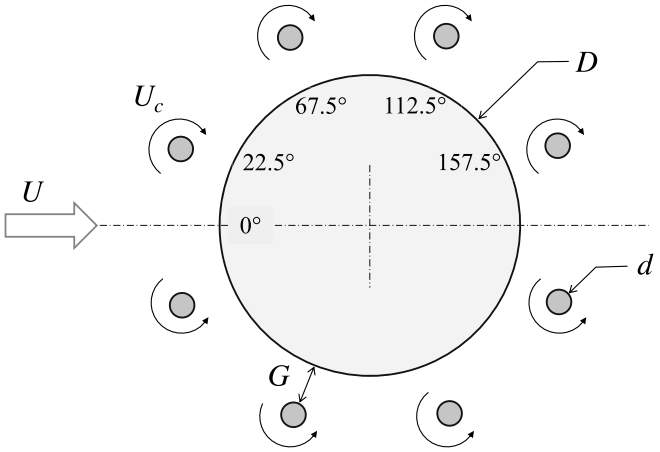

Fig. 1. Geometrical parameters for the main cylinder with eight wake-control cylinders. Flow approaching in the direction of the arrow; direction of rotation is marked on each cylinder.

3. Numerical method

Numerical simulations of the flow have been carried out employing the commercial code ANSYS Fluent (version 13.0). The flow was governed by the Navier–Stokes equations, which were considered here as incompressible and two-dimensional. The unsteady Navier–Stokes equations for the conservation of mass and momentum in the integral form were given by

$$\int_S \vec{u}.\vec{n}\mathrm{d}S = 0 \tag{1}$$

and

$$\int_\Omega \frac{\partial \rho \vec{u}}{\partial t} d\Omega + \int_S \rho \vec{u}(\vec{u}\cdot\vec{n})dS = \int_S \left(-p\vec{n}\right) dS + \int_S (\bar{\bar{\tau}}\cdot\vec{n})dS, \tag{2}$$

where the viscous stress tensor for Newtonian fluid was

$$\bar{\bar{\tau}} = \mu\left[\left(\nabla\vec{u} + \nabla\vec{u}^{\mathrm{T}}\right) - \frac{2}{3}(\nabla\cdot\vec{u})I\right]. \tag{3}$$

In the equations above, $\vec{u}$ is the flow speed, p the static pressure, ρ is the specific mass of fluid, μ is the dynamic viscosity, t is the time, Ω represents the control volume of the system and S denotes its external surfaces, whose outward unit normal is $\vec{n}$.

The equations were discretised by a cell-centred finite-volume method. The fluid domain was divided into a large number of discrete control volumes by means of a computational mesh. The resulting discretised equations were solved sequentially based on an implicit pressure-based scheme. In order to deal with the pressure–velocity coupling, the pressure-based algorithm PISO was employed due to its efficient iterative method for unsteady problems, the scheme is fully described in Versteeg and Malalasekera (2007).

In order to obtain the pressure on the faces of the control volume, an interpolation scheme based on a "staggered" control volume arrangement was employed (known in Fluent as PRESTO, PREssure Staggering Option). The staggered-grid scheme procedure is also described in Versteeg and Malalasekera (2007). An upwind second-order spatial differencing method was applied for the convective terms (Barth and Jespersen, 1989) and the diffusive terms were discretised by a central differencing scheme. The solution was time-advanced using an implicit second-order accurate scheme that employed three time levels incorporated within the PISO algorithm (Versteeg and Malalasekera, 2007). All the equations were solved iteratively, for a given time-step, until the convergence criterium was met: all residuals for each algebraic equation were less than 10^{-4} and 20 internal iterations per time step.

3.1. Computational domain

The cylinders were surrounded by a rectangular computation domain with upstream, lateral and downstream boundaries located respectively at 8D, 8D and 30D from the centre of the main cylinder, as shown in Fig. 2. The size of the computational domain was verified so that the flow around the cylinder was not too much influenced by the boundaries. It is well known that the size of the domain influences Strouhal number and other hydrodynamic coefficients (Behr et al.,

Please cite this article as: G.R.S. Assi, R.M. Orselli and M. Silva-Ortega, Control of vortex shedding from a circular cylinder surrounded by eight rotating wake-control cylinders at Re=100. Journal of Fluids and Structures (2019), https://doi.org/10.1016/j.jfluidstructs.2019.03.003.

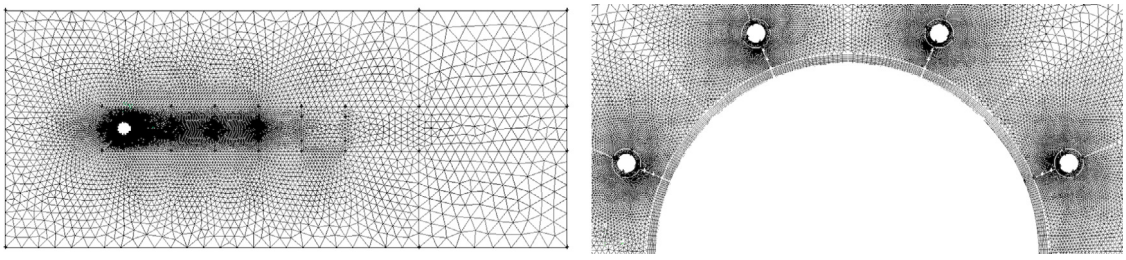

Fig. 2. The wider numerical domain (left) and a detail of the mesh around the control cylinders (right).

Table 1
Comparison of drag and lift coefficients.

	St	$\overline{C}_D$	$\hat{C}_L$
Present work	0.175	1.401	0.227
Blanchard et al. (2019)	0.170	1.392	0.242

1995). Nevertheless, the size of the employed domain was considered a good balance between computational costs and accuracy of the physical phenomenon. Numerical domains of a similar size or smaller have been successfully employed by Mittal (2001), Young et al. (2001) and Goodarzi and Dehkordi (2017) to investigate analogous problems.

The two-dimensional, finite-volume mesh (with 89,310 cells) was fine enough to resolve the details of the flow near the walls. A structured finite-volume mesh was employed close to the main cylinder and the small cylinders. Mesh-convergence tests have been carried out until a suitable final mesh was found. (Details of this validation exercise will not be reported here for brevity.) Simulations run for enough time to gather at least six cycles of vortex shedding in a fully developed wake.

A no-slip condition was specified for the velocity on the surface of all bodies and free-stream values were assigned to the velocity at the upstream boundary. On the upper and lower boundaries, the component of velocity normal to and the component of the stress vector along these boundaries were prescribed to be zero. At the downstream boundary, an outflow boundary condition was employed, which prescribes all variables' normal gradient to zero.

The direction of the incoming flow and the direction of the rotation of the control cylinders are marked in Fig. 1. The control cylinders were distributed so that there would be no control cylinder positioned at the frontal stagnation region, thus avoiding any asymmetry of the flow around the body. (Future work should concentrate on that arrangement.) The rotation speed (U_c/U) of the control cylinders was imposed at each case being simulated. Coefficients of lift (C_L) and drag (C_D) were determined by integrating the pressure field and viscous forces on the walls around the main cylinder and the control cylinders. The force coefficients per unit length were normalised by $\frac{1}{2}\rho U^2 D$, always in reference to the diameter D of the main cylinder (even if the body in question was a small control cylinder).

4. Results and discussion

4.1. Reference: a bare cylinder

The flow around a bare cylinder (without control cylinders) at $Re = 100$ was simulated in order to validate the numerical model and domain as well as to serve as a reference for comparison. From the time series of lift and drag coefficients shown in Fig. 3(a), a steady state regime of vortex shedding was achieved after 70 non-dimensional time units from the beginning of the simulation. The steady-state Strouhal number (defined as $St = f_s D/U$, where f_s is the frequency of vortex shedding), the mean drag coefficient ($\overline{C}_D$) and the fluctuation of the lift coefficient ($\hat{C}_L$, calculated as the root mean square of lift) are presented in Table 1 in comparison with another two-dimensional numerical simulation from the literature. These values were also in good agreement with Meneghini et al. (2001), Norberg (2003), Rajani et al. (2009) and Muddada and Patnaik (2010).

Fig. 3 also presents the vorticity field and streamlines downstream of the bare cylinder for an instant once the periodic regime of vortex shedding had been established. A typical Karman vortex street – with two single vortices shed per cycle – is clearly identified from the vorticity contours, while the region of separated flow at the base of the cylinder is highlighted by the streamlines.

4.2. With rotating control cylinders

The rotating control cylinders were placed close enough to the wall to interact with the boundary layer of the main cylinder, but not necessarily immersed in it. Fig. 4 illustrates the velocity profiles of the flow around the bare cylinder,

Please cite this article as: G.R.S. Assi, R.M. Orselli and M. Silva-Ortega, Control of vortex shedding from a circular cylinder surrounded by eight rotating wake-control cylinders at Re=100. Journal of Fluids and Structures (2019), https://doi.org/10.1016/j.jfluidstructs.2019.03.003.

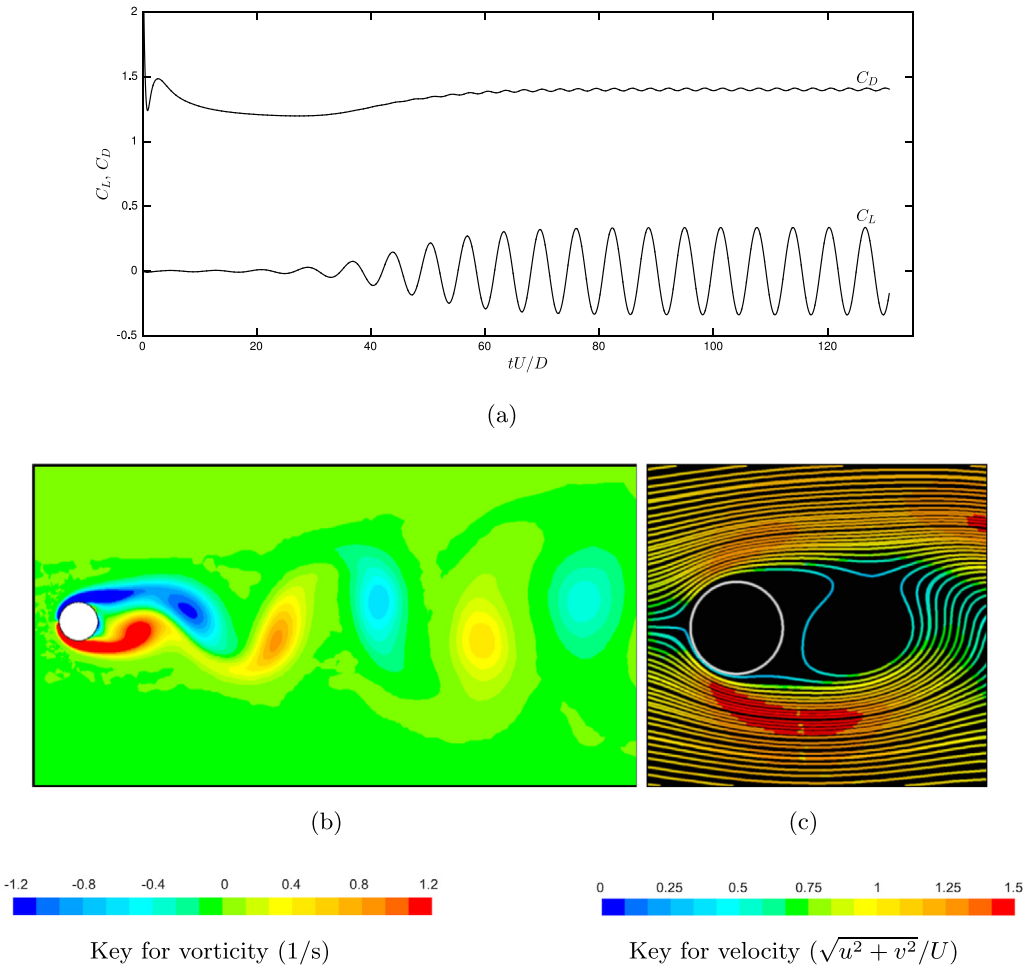

Fig. 3. (a) Time series of C_L and C_D, (b) instantaneous vorticity contours and (c) streamlines for the flow around a bare cylinder.

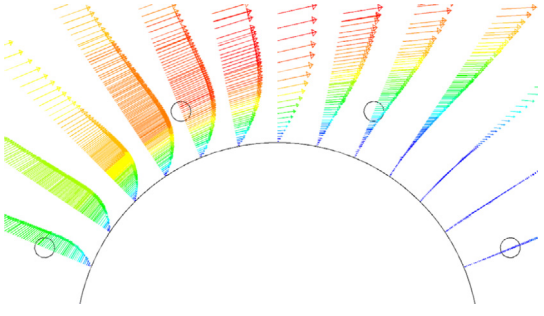

Fig. 4. Details of the velocity profile in the boundary layer around the bare cylinder (coloured by velocity magnitude; key in Fig. 3). Flow is from left to right.

highlighting the shear profile in the boundary layer and the eventual locations and diameter of the control cylinders (marked by the corresponding circles at $G/D = 0.1$).

The rotation of the control cylinders (U_c/U) was increased in steps. At the beginning of the simulation ($tU/D = 0$), U_c/U was set to 0. Once a steady state regime of vortex shedding had been reached, the simulation would be left to run for several cycles of vortex shedding before the parameter was changed to the next step $U_c/U = 1$. Once more, after several cycles of stablished vortex shedding, U_c/U was increased to the next step, and so on, until $U_c/U = 6$. Following this method, a transient regime appeared after each change in U_c/U, the convergence time was reduced, but each simulation

Please cite this article as: G.R.S. Assi, R.M. Orselli and M. Silva-Ortega, Control of vortex shedding from a circular cylinder surrounded by eight rotating wake-control cylinders at Re=100. Journal of Fluids and Structures (2019), https://doi.org/10.1016/j.jfluidstructs.2019.03.003.

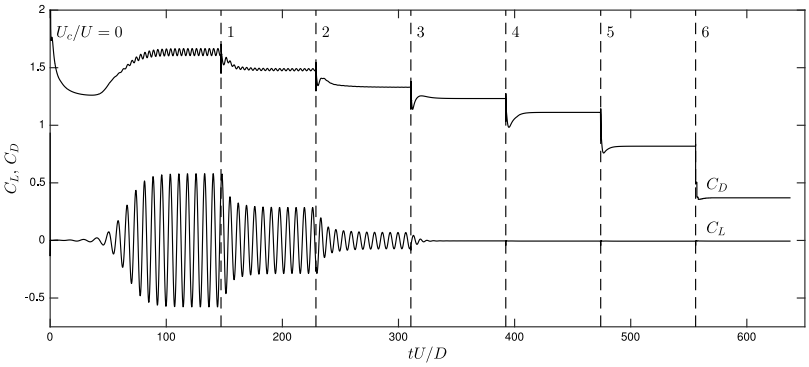

Fig. 5. Time series of C_L and C_D for a cylinder with 8 rotating control cylinders. Coefficients measured on the main cylinder alone.

carried information from the previous state. This procedure, also employed by Mittal (2001), produced the time series of C_D and C_L presented in Fig. 5, where the dashed lines mark the transitions in U_c/U.

Fig. 6 presents the instantaneous vorticity contours and the corresponding streamlines for the flow around a cylinder with 8 rotating control cylinders for $U_c/U = 0$ to 6. At $U_c/U = 0$ the wake pattern looked similar to that of a bare cylinder, as shown in Fig. 3, except that the presence of the 8 non-rotating control cylinders made the wake wider than that of the bare cylinder.

Reynolds number based on the diameter of the control cylinders was $Re_c = 5$, which was below the typical value of $Re_c = 46$ from which shear layer instability should trigger the onset of vortex shedding for the individual control cylinders. Therefore, no independent vortex-shedding was observed from the control cylinders, hence the vortex wake was produced by the main and the control cylinders combined as a single body.

As shown by the streamlines, the region of separated flow (associated with the recirculation bubble) downstream of the main cylinder was reduced as U_c/U was increased. The strength of convected vortices also decreased as U_c/U increased at the same time that the vortex formation length was increased, showing that the separated shear layers were interacting further downstream to generate a weaker wake. Eventually for $U_c/U \geq 3$, the interaction between the separated shear layers was so much reduced that no alternating vortex shedding was noticed in the wake downstream of the main cylinder. This was also accompanied by a narrowing of the wake and a consequent increase in Strouhal number.

4.3. Fluid forces

The suppression of the wake as U_c/U was increased was followed by changes in the fluid forces acting on the body, which was evident from the time series of C_L and C_D measured on the main cylinder alone (Fig. 5). The RMS of fluctuating lift coefficient decreased as the rotation of the control cylinders was increased. A periodic fluctuation of C_L was clear for U_c/U between 0 and 2, but disappeared for $U_c/U \geq 3$ when vortex shedding was completely suppressed.

The drag coefficient followed the same behaviour. The mean drag coefficient was found to be $\overline{C}_D = 2.1$ for $U_c/U = 0$, higher than that experienced by an isolated cylinder, since the presence of the static control cylinders contributed to the enhancement of the wake and increased drag on the main cylinder. $\overline{C}_D$ was reduced as the wake got weaker for higher U_c/U. The minimum $\overline{C}_D \approx 0.4$ (with $\hat{C}_L \approx 0$) was obtained for $U_c/U = 5$, which was much lower than the $\overline{C}_D = 1.4$ found for the bare cylinder (Fig. 3(a)). For the highest $U_c/U = 6$, the system reached the lowest drag recorded at $\overline{C}_D \approx 0.37$ (considerably below that of the bare cylinder), but a local minimum value may still be waiting ahead.

Fig. 7(a) presents the mean drag coefficient ($\overline{C}_D$) compared with the reference $\overline{C}_D = 1.40$ for that of the bare cylinder. White symbols refer to coefficients measured on the main cylinder alone, while black symbols refer to the system as a whole (main cylinder plus wake-control cylinders). When $\overline{C}_D$ was measured on the whole system (black symbols) a very interesting behaviour stood out: for higher U_c/U the whole system was able to achieve considerably less drag than the main cylinder alone. In fact, for the case at $U_c/U = 6$ the mean drag was even found to be negative ($\overline{C}_D \approx -0.1$). The interaction of the rotating control cylinders with the flow past the main body generated force in the opposite direction of the incoming flow. While the main cylinder was always under positive drag, the force on the control cylinders can balance or overtake that of the main body, generating a net negative drag (a small propulsion, or thrust) for the whole system.

So far, it is impossible to conclude if the total $\overline{C}_D$ will continue to drop for higher rotation speeds. But the fact that the rotating cylinders were not only able to reduce but to overcome the overall drag of the system is quite remarkable. Nevertheless, we conclude that the negative term of the total drag was indeed coming from the rotating control cylinders.

Now turning to the absolute mean lift coefficient in Fig. 7(b). Since the cylinders on opposite sides of the body were rotating at opposite directions – and since positive C_L is defined in the cross-flow direction pointing upwards in Fig. 1 –

Please cite this article as: G.R.S. Assi, R.M. Orselli and M. Silva-Ortega, Control of vortex shedding from a circular cylinder surrounded by eight rotating wake-control cylinders at Re=100. Journal of Fluids and Structures (2019), https://doi.org/10.1016/j.jfluidstructs.2019.03.003.

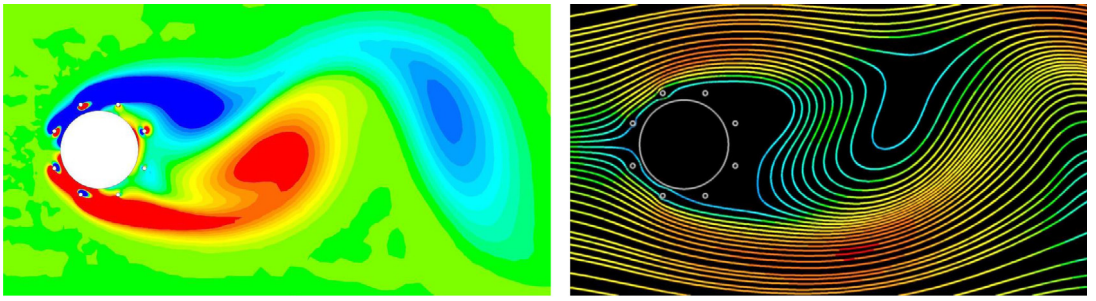

(a) $U_c/U = 0$

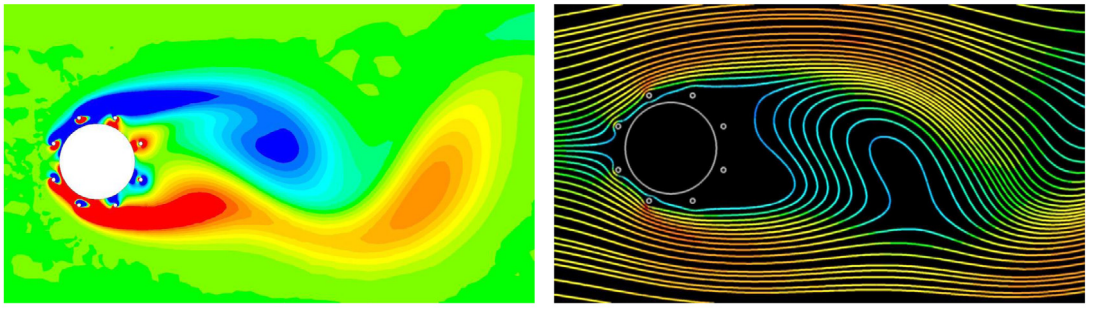

(b) $U_c/U = 1$

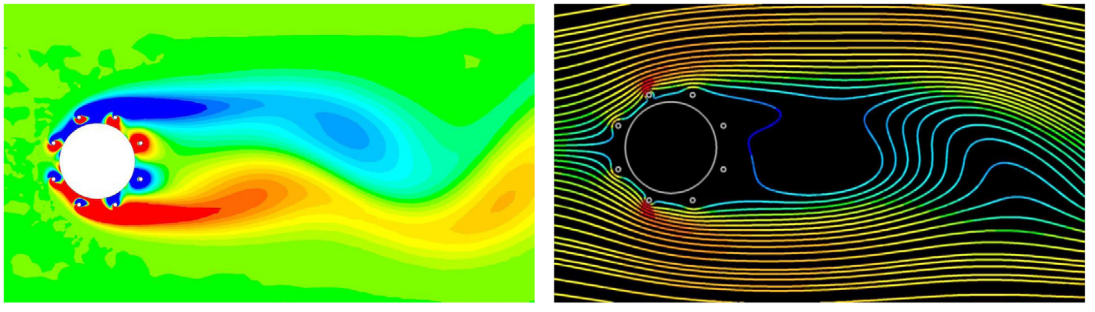

(c) $U_c/U = 2$

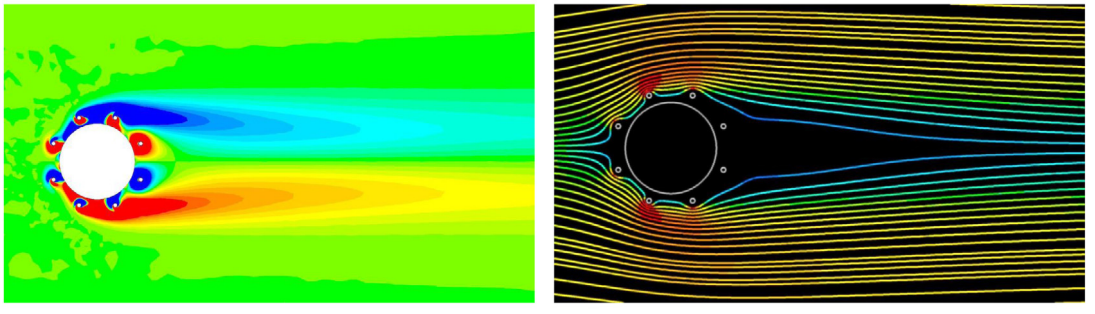

(d) $U_c/U = 3$

Fig. 6. Instantaneous vorticity contours (left column) and corresponding streamlines (right column) of the flow around a cylinder with 8 rotating control cylinders ($U_c/U = 0$ to 6). Coloured by vorticity and velocity magnitude, respectively.

we shall consider the absolute value of lift. Fig. 7(b) presents lift also divided in two terms: for the main cylinder alone and for the absolute portion acting on the control cylinders (therefore $|\overline{C}_L|$).

Please cite this article as: G.R.S. Assi, R.M. Orselli and M. Silva-Ortega, Control of vortex shedding from a circular cylinder surrounded by eight rotating wake-control cylinders at Re=100. Journal of Fluids and Structures (2019), https://doi.org/10.1016/j.jfluidstructs.2019.03.003.

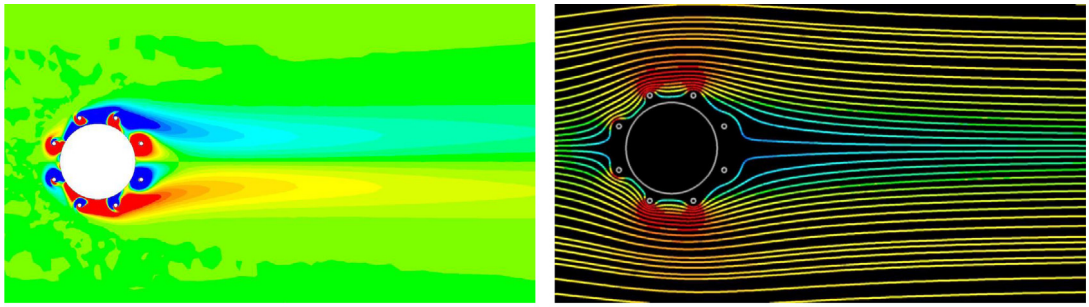

(e) $U_c/U = 4$

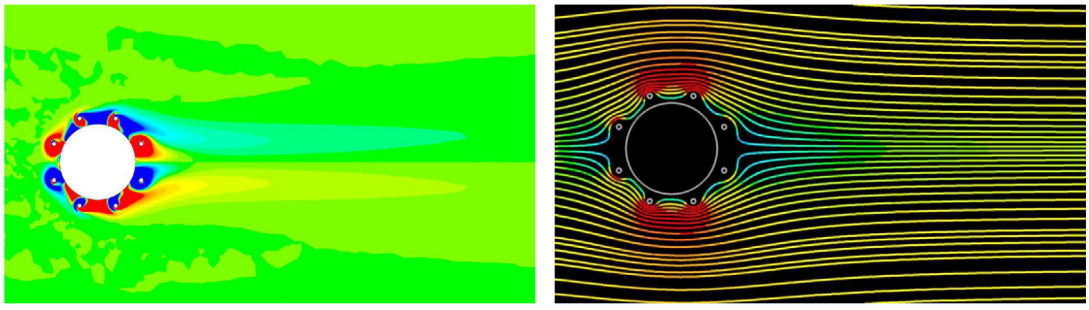

(f) $U_c/U = 5$

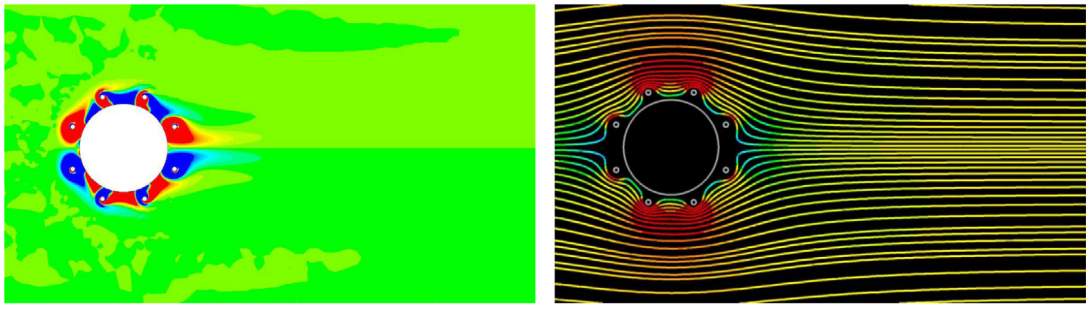

(g) $U_c/U = 6$

Key for vorticity (1/s)

Key for velocity ($\sqrt{u^2 + v^2}/U$)

Fig. 6. (*continued*).

As expected, the main cylinder alone presented $\overline{C}_L \approx 0$ due to the symmetry of the flow. (Any difference from zero was due to not having an integer number of cycles while taking the average of the time series.) The control cylinders, on the other hand, appeared to sum up a rather high value of $|\overline{C}_L|$, which increased continuously with U_c/U. The four control cylinders on the top side of the main cylinder produced a net lift pushing upwards; the four control cylinders on the bottom side produce a net lift of the same magnitude pushing downwards. For this reason, $|\overline{C}_L|$ is presented in Fig. 7(b) as referring to the mean value of the cylinders on each side of the main body. If both terms were to be added, the net lift on the top side would cancel out the net lift on the bottom side, hence the total lift experienced by the whole system would also be $\overline{C}_L \approx 0$, as seen in Fig. 7(b).

It was shown that the 8 wake-control cylinders were indeed experiencing a considerable amount of fluid forces, either to generate negative drag or to generate lift pointing away from the centreline of the wake. A control strategy could take advantage of this net lift by rotating only the control cylinders on one side of the body, for example, to produce lift to maneuver the system. More advanced control strategies could consider the independent rotation of the control cylinders

Please cite this article as: G.R.S. Assi, R.M. Orselli and M. Silva-Ortega, Control of vortex shedding from a circular cylinder surrounded by eight rotating wake-control cylinders at Re=100. Journal of Fluids and Structures (2019), https://doi.org/10.1016/j.jfluidstructs.2019.03.003.

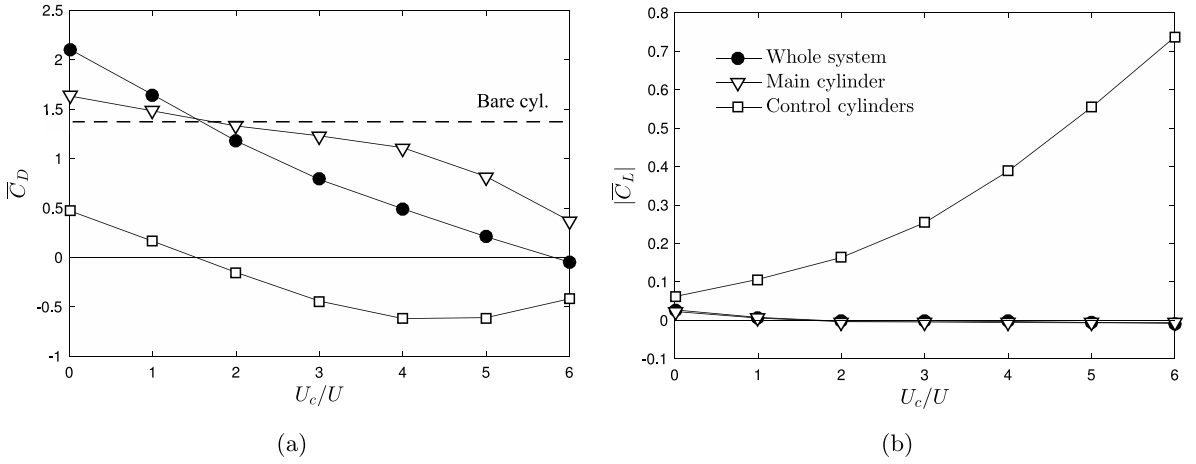

Fig. 7. (a) Mean drag and (b) absolute mean lift for the case with 8 control cylinders.

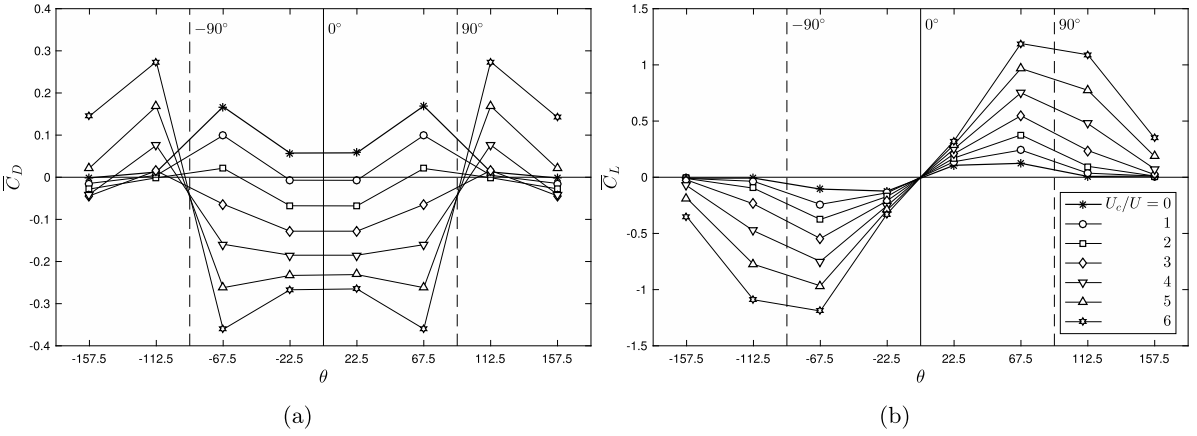

Fig. 8. Contribution of each control cylinder to the total (a) drag and (b) lift of the system.

to generate a useful force in a desired direction. To pave the way, we shall now investigate the contribution of each control cylinder independently.

4.4. Force acting on each control cylinder

Fig. 8 presents the mean drag and mean lift coefficients measured for each of the 8 control cylinders around the main body for various rotation speeds. The angular position (θ) of the control cylinders is that shown in Fig. 1.

When $U_c/U = 0$ none of the control cylinders experienced negative drag (Fig. 8(a)). But as soon as they started to rotate some of the control cylinders contributed with negative drag, especially those located at the front of the body (between the $\pm 90°$ dashed lines) where the flow had not yet separated. For the highest $U_c/U = 6$ the control cylinders located at the front produced so much negative drag that they were able to balance off the positive drag experienced by the other control cylinders and the main cylinder. It becomes clear that the control cylinders located at $\pm 67.5°$ were the ones that contributed the most to reduce the total drag of the system. The next cylinders downstream, located at $\pm 112.5°$, interacted with the separated shear layers and produce positive drag for most cases.

Fig. 8(b) presents the contribution of each cylinder towards lift. It is clear that all cylinders on the top side of the body produced positive lift (pointing upwards), while all cylinders on the bottom side produce negative lift. The control cylinders located at $\pm 67.5°$ were the ones with the strongest lift, reaching $|\overline{C}_L| \approx 1.2$ for the highest rotation of $U_c/U = 6$.

Finally, Fig. 9 presents the resultant force in terms of a vector diagram for each of the 8 control cylinders for $U_c/U = 0$ to 6. The resultant vector for the forces measured on the main cylinder alone are also presented as a black arrow at the centre of the main body. The grey arrow represents the resultant vector for the system as a whole.

At $U_c/U = 0$ the control cylinders generated positive drag, except for the cylinder immersed in the recirculation region of the near wake. Adding that to the drag of the main cylinder results in the highest value of $\overline{C}_D$ experienced by the system.

Please cite this article as: G.R.S. Assi, R.M. Orselli and M. Silva-Ortega, Control of vortex shedding from a circular cylinder surrounded by eight rotating wake-control cylinders at Re=100. Journal of Fluids and Structures (2019), https://doi.org/10.1016/j.jfluidstructs.2019.03.003.

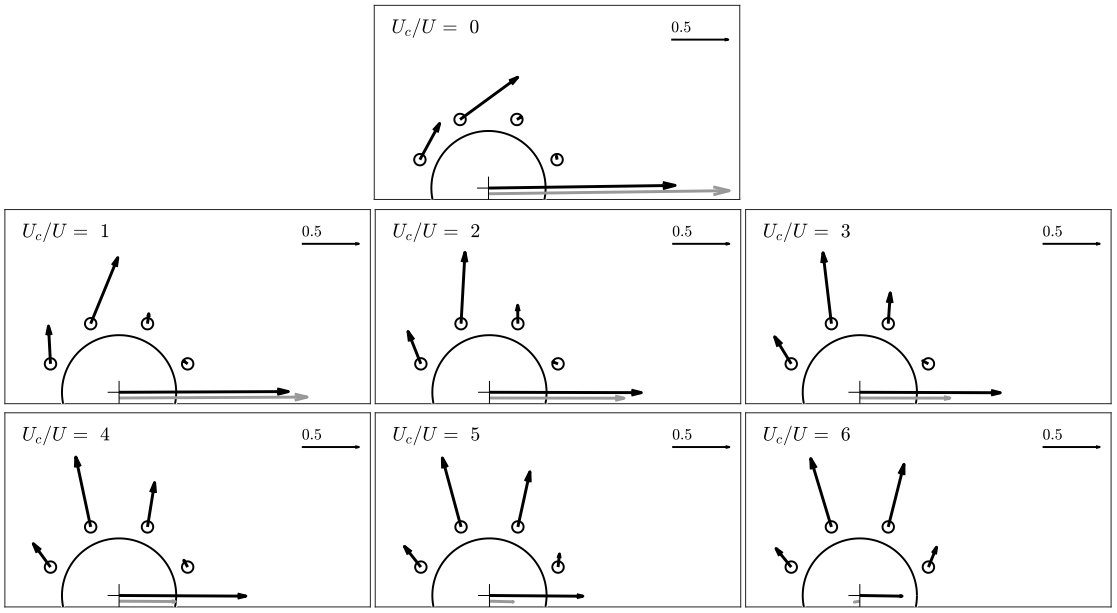

Fig. 9. Resultant force coefficients (shown as vector diagrams) on each control cylinder, main cylinder alone (black arrow) and the system as a whole (grey arrow). Direction of the flow is from left to right.

As U_c/U was increased the drag of the main cylinder was gradually reduced, and drag on the control cylinders (especially on those at the front) became negative, reducing $\overline{C}_D$ of the whole system until it got negative for $U_C/U = 6$.

As vortex-shedding was eliminated for $U_c/U \geq 3$ the direction of the resultant vectors of the control cylinders did not change much, but they only increased their magnitude with increasing rotation speed. Such a large lift-to-drag ratio could prove to be useful for other control applications such as dynamic positioning of offshore floating units.

4.5. Driving power

One final important question regards the amount of energy spent to rotate the control cylinders compared with the energy saved due to drag reduction. Following the model for energy efficiency proposed by Shukla and Arakeri (2013), the power P_n needed to rotate a single control cylinder at a tangential velocity U_c is that required to overcome the total effect of shear stresses on its wall, which is integrated around the diameter d, hence

$$P_n = U_c \frac{d}{2} \int_0^{2\pi} \tau_{\theta_c} \, \mathrm{d}\theta_c, \tag{4}$$

where τ_{θ_c} is the local shear stress on the wall of the control cylinder. Adding up the contributions of all the N control cylinders results in

$$C_N = \sum_n^N \frac{P_n}{\rho U^3 D/2}, \tag{5}$$

the coefficient of power spent to rotate all the control cylinders of a system at the same tangential velocity U_c.

Finally, the total power-loss coefficient

$$C_{PL} = \overline{C}_D + C_N \tag{6}$$

of the system is simply obtained by adding the total drag of the system ($\overline{C}_D$) to the energy spent to rotate the N control cylinders (C_N). In general terms, the power-loss coefficient is a means to evaluate the energy efficiency of the system regarding the amount of energy spent to drive the control cylinders and the energy lost due to the drag the system generates.

Fig. 10 presents C_{PL} decomposed in C_N and $\overline{C}_D$ as a function of U_c/U. As expected, for non-rotating control cylinders ($U_c/U = 0$) all the power-loss of the system was due to drag, which was slightly higher than that experienced by a bare cylinder. As rotation speed was increased, an increasing fraction of the power was lost to the rotation of the control cylinders, but the resulting reduction of the overall $\overline{C}_D$ dominates the behaviour of C_{PL}.

Coincidentally or not, it is interesting to note that the condition for the suppression of vortex shedding (shaded area in Fig. 10) is somewhat related to when C_N is greater than $\overline{C}_D$. Nevertheless, the minimum C_{PL} for when suppression is

Please cite this article as: G.R.S. Assi, R.M. Orselli and M. Silva-Ortega, Control of vortex shedding from a circular cylinder surrounded by eight rotating wake-control cylinders at Re=100. Journal of Fluids and Structures (2019), https://doi.org/10.1016/j.jfluidstructs.2019.03.003.

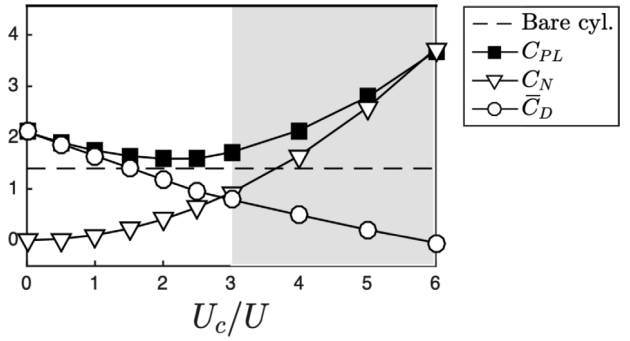

Fig. 10. Decomposition of the power-loss coefficient (C_{PL}). Area shaded in grey represents when vortex shedding was suppressed. The horizontal, dashed lines represent $\overline{C}_D = 1.4$ for a bare cylinder.

achieved (at $U_c/U = 3$) is still greater than the mean drag for a bare cylinder, at least for this specific condition of Re, G/D, d/D, etc.

As examples, consider two applications: (1) If the objective is to suppress the fluctuating forces caused by vortex shedding with minimal energy input, U_c/U would be set around 3. (2) But if the objective is to minimise drag (or maybe generate useful thrust) at the cost of spending more energy, than the user would set higher rotation speeds.

5. Final remarks

Two-dimensional simulations of the flow offer a simplified view of the phenomena occurring in the wake, which is indeed much more complex and rich in three-dimensionalities, as carefully exposed by Williamson (1996). A parametric investigation, however, would be extremely expensive in terms of the computational effort required to model the three-dimensional flow at higher Re (Assi et al., 2018, for example). Therefore, simplified simulations still hold their place as a powerful and feasible tool to understand the hydrodynamic mechanisms at the beginning of the instabilities ($Re = 100$). Perhaps the most useful point in the present study is that it helps us to formulate the correct questions concerning wake stability and flow control in such a simple geometry, but with too many parameters in hand.

Now, thinking in terms of practical applications (especially related to offshore and wind engineering), there are situations in which fitting 8 control cylinders is better (or actually necessary) than fitting only 2 or 4. If the direction of the incoming flow is not known or changes with time, for example, a system with 8 control cylinders would appear to be "more omnidirectional" to the flow than the previous cases. Of course a case with 16 control cylinders would be hypothetically even "more omnidirectional" (keeping this term with quotation marks as omnidirectionality is not quantifiable), but that would be just another step in one of the significant parameters.

Of course there are infinite possibilities to arrange the rotating control cylinders around the main cylinder. The present work was never intended to find an optimal solution, but simply to be a parametric study. (Refer to Patino et al. (2015) and Meliga et al. (2014) for good optimisation studies regarding the location of interfering control cylinders.) Our initial restriction, however, was to reduce the number of geometric parameters for axisymmetric arrays of control cylinders. The universe of parameters for an optimisation study is so vast that a robust optimisation method must be considered to tackle the problem. With as many significant parameters identified in this work (N, d/D, G/D, U_c/U, angle of incidence in relation to the upcoming flow) as those not concerned in the investigation (control cylinders do not need to have the same diameter, or to be equally spaced, or to rotate at the same speed and direction, or to be at same distance from the centre...), one may see the possibilities are endless, making it a very exciting, non-linear problem for someone focusing on optimisation.

6. Conclusion

In the present work, the flow control past a circular cylinder surrounded by 8 rotating wake-control cylinders has been studied by means of numerical simulations at $Re = 100$. The control cylinders were able to suppress the vortex shedding mechanism of the main cylinder for rotations greater than $U_c/U = 3$.

Drag on the system was reduced as a consequence of the elimination of the Karman vortex street, but it appeared that a local minimum was not reached yet within the range of this investigation. Mean drag experienced by the control cylinders can be negative and, for higher rotation speeds, stronger in magnitude than the positive drag experienced by the main body. Indeed, the lowest drag of $\overline{C}_D \approx -0.1$ was observed for $U_c/U = 6$. It s not clear if $\overline{C}_D$ tends toward a minimum value or will it keep decreasing with increasing rotation speeds. On the other hand, the power spent to rotate the 8 control cylinders appear to be higher than the power loss associated with the mean drag of the bare cylinder.

The control cylinders also experience high lift, what can be useful if a control strategy requires to control the lateral force on the body. Such forces originate in the interaction of certain control cylinders with the attached boundary layers.

Please cite this article as: G.R.S. Assi, R.M. Orselli and M. Silva-Ortega, Control of vortex shedding from a circular cylinder surrounded by eight rotating wake-control cylinders at Re=100. Journal of Fluids and Structures (2019), https://doi.org/10.1016/j.jfluidstructs.2019.03.003.

The two-dimensional computations set an upper bound on the control effectiveness of the rotating cylinders. It is expected that the actual behaviour of such open-loop control strategies will depend significantly on three-dimensional effects and Reynolds number (among other factors). Future numerical and experimental investigation should concentrate on that.

Acknowledgements

MSO and RMO are grateful to CAPES Brazilian Ministry of Education. GRSA acknowledges the support of FAPESP, Brazil (2011/00205-6, 2014/50279-4), CNPq, Brazil (306917/2015-7) and the Brazilian Navy.

References

Assi, G.R.S., Bearman, P.W., Kitney, N., 2009. Low drag solutions for suppressing vortex-induced vibration of circular cylinders. J. Fluids Struct. 25, 666–675.
Assi, G.R.S., Bearman, P.W., Kitney, N., Tognarelli, M., 2010. Suppression of wake-induced vibration of tandem cylinders with free-to-rotate control plates. J. Fluids Struct. 26, 1045–1057.
Assi, G.R.S., Orselli, R.M., Silva-Ortega, M., 2018. Suppression of vortex shedding with rotating wake-control cylinders: numerical investigation at a moderate Reynolds number. In: ASME (Ed.), Proceedings of OMAE 37th International Conference on Ocean, Offshore and Arctic Engineering, No. OMAE2018-78316.
Barth, T.J., Jespersen, D.C., 1989. The design and application of upwind schemes on unstructured meshes, AIAA PAPER 89-0366.
Bearman, P.W., 1984. Vortex shedding from oscillating bluff bodies. Annu. Rev. Fluid Mech. 16, 195–222.
Behr, M., Hastreiter, D., Mittal, S., Tezduyar, T., 1995. Incompressible flow past a circular cylinder: dependence of the computed flow field on the location of the lateral boundaries. Comput. Methods Appl. Mech. Engrg. 123 (1), 309–316.
Blanchard, A., Bergman, L.A., Vakakis, A.F., 2019. Nonlinear Dyn. http://dx.doi.org/10.1007/s11071-019-04775-3.
Cattafesta, L., Sheplak, M., 2011. Actuators for active flow control. Annu. Rev. Fluid Mech. 43, 247–272.
Choi, H., Jeon, W.-P., Kim, J., 2008. Control of flow over a bluff body. Annu. Rev. Fluid Mech. 40, 113–139.
Gad-El-Hak, M., 2000. Flow Control: Passive, Active, and Reactive Flow Management. Cambrigde University Press.
Gerrard, J., 1966. The mechanics of the formation region of vortices behind bluff bodies. J. Fluid Mech. 25, 401–413.
Goodarzi, M., Dehkordi, E.K., 2017. Geometrical parameter analysis on stabilizing the flow regime over a circular cylinder using two small rotating controllers. Comput. & Fluids 145, 129–140.
Jimenez-Gonzalez, J.I., Huera-Huarte, F.J., 2017. Experimental sensitivity of vortex-induced vibrations to localized wake perturbations. J. Fluids Struct. 74, 53–63.
Korkischko, I., Meneghini, J., 2012. Suppression of vortex-induced vibration using moving surface boundary-layer control. J. Fluids Struct. 34, 259–270.
Meliga, P., Boujo, E., Pujals, G., Gallaire, F., 2014. Sensitivity of aerodynamic forces in laminar and turbulent flow past a square cylinder. Phys. Fluids 26 (104101).
Meneghini, J., Saltara, F., Siqueira, C., Ferrari, J., 2001. Numerical simulation of flow interference between two circular cylinders in tandem and side-by-side arrangements. J. Fluids Struct. 15 (2), 327–350.
Mittal, S., 2001. Control of flow past bluff bodies using rotating control cylinders. J. Fluids Struct. 15 (2), 291–326.
Mittal, S., 2003. Flow control using rotating cylinders: effect of gap. J. Appl. Mech. 70 (5), 762–770.
Mittal, S., Raghuvanshi, A., 2001. Control of vortex shedding behind circular cylinder for flows at low Reynolds numbers. Internat. J. Numer. Methods Fluids 35 (4), 421–447.
Modi, V., 1997. Moving surface boundary-layer control: a review. J. Fluids Struct. 11 (6), 627–663.
Muddada, S., Patnaik, B., 2010. An active flow control strategy for the suppression of vortex structures behind a circular cylinder. Eur. J. Mech. B/Fluids 29 (2), 93–104.
Norberg, C., 2003. Fluctuating lift on a circular cylinder: review and new measurements. J. Fluids Struct. 17, 57–96.
Patino, G., Silva-Ortega, M., Gioria, R.S., Assi, G.S.R., Meneghini, J.R., 2015. Investigation of circular cylinder VIV passive control device using flow sensitivity analysis. In: 6th International Symposium on Bifurcations and Instabilities in Fluid Dynamics - BIFD2015.
Patnaik, B., Wei, G., 2002. Controlling wake turbulence. Phys. Rev. Lett. 88, 1–4.
Rajani, B., Kandasamy, A., Majumdar, S., 2009. Numerical simulation of laminar flow past a circular cylinder. Appl. Math. Model. 33, 1228–1247.
Rashidi, S., Hayatdavoodi, M., Esfahani, J.A., 2016. Vortex shedding suppression and wake control: A review. Ocean Eng. 126, 57–80.
Schulmeister, J., 2012. Flow separation control with rotating cylinders (Master's thesis,), Massachusetts Institute of Technology.
Schulmeister, J.C., Dahl, J.M., Weymouth, G.D., Triantafyllou, M.S., 2017. Flow control with rotating cylinders. J. Fluid Mech. 825, 743–763.
Shukla, R.K., Arakeri, J.H., 2013. Minimum power consumption for drag reduction on a circular cylinder by tangential surface motion. J. Fluid Mech. 715, 597–641.
Silva-Ortega, M., 2015. Suppression of vortex-induced vibration of a circular cylinder with fixed and rotating control cylinders (Master's thesis,), Universidade de São Paulo.
Silva-Ortega, M., Assi, G.R.S., 2017a. Flow-induced vibration of a circular cylinder surrounded by two, four and eight wake-control cylinders. Exp. Therm Fluid Sci. 85, 354–362.
Silva-Ortega, M., Assi, G.R.S., 2017b. Suppression of the vortex-induced vibration of a circular cylinder surrounded by eight rotating wake-control cylinders. J. Fluids Struct. 74, 401–412.
Silva-Ortega, M., Assi, G.R.S., 2018. Hydrodynamic loads on a circular cylinder surrounded by two, four and eight wake-control cylinders. Ocean Eng. 153, 345–352.
Strykowski, P.J., Sreenivasan, K.R., 1990. On the formation and suppression of vortex shedding at low Reynolds numbers. J. Fluid Mech. 218, 71–107.
Versteeg, H.K., Malalasekera, W., 2007. An Introduction to Computational Fluid Dynamics: The Finite Volume Method. Pearson Education.
Williamson, C.H.K., 1996. Vortex dynamics in the cylinder wake. Annu. Rev. Fluid Mech. 28 (1), 477–539.
Wu, H., Sun, D., Lu, L., Teng, B., Tang, G., Song, J., 2012. Experimental investigation on the suppression of vortex-induced vibration of long flexible riser by multiple control rods. J. Fluids Struct. 30, 115–132.
Young, D., Huang, J., Eldho, T., 2001. Simulation of laminar vortex shedding flow past cylinders using a coupled BEM and FEM model. Comput. Methods Appl. Mech. Engrg. 190 (45), 5975–5998.
Zdravkovich, M.M., 1981. Review and classification of various aerodynamic and hydrodynamic means for suppressing vortex shedding. J. Wind Eng. Ind. Aerodyn. 7, 145–189.
Zhu, H., Gao, Y., 2017. Vortex-induced vibration suppression of a main circular cylinder with two rotating control rods in its near wake: effect of the rotation direction. J. Fluids Struct. 74, 469–491.
Zhu, H., Yao, J., Ma, Y., Zhao, H., Tang, Y., 2015. Simultaneous CFD evaluation of VIV suppression using smaller control cylinders. J. Fluids Struct. 57, 66–80.

Please cite this article as: G.R.S. Assi, R.M. Orselli and M. Silva-Ortega, Control of vortex shedding from a circular cylinder surrounded by eight rotating wake-control cylinders at Re=100. Journal of Fluids and Structures (2019), https://doi.org/10.1016/j.jfluidstructs.2019.03.003.